Novel Zn9-cluster compounds RE2Zn6Ge3 (RE: La, Ce, Pr, Nd, Sm, Gd): crystal structure and physical properties

2003 J. Phys.: Condens. Matter 15 3053

(http://iopscience.iop.org/0953-8984/15/19/308)

INSTITUTE OF PHYSICS PUBLISHING JOURNAL OF PHYSICS: CONDENSED MATTER

J. Phys.: Condens. Matter **15** (2003) 3053–3067 PII: S0953-8984(03)58520-4

Novel Zn_9-cluster compounds $RE_2Zn_6Ge_3$ (RE: La, Ce, Pr, Nd, Sm, Gd): crystal structure and physical properties*

A Grytsiv[1], E Bauer[2], St Berger[2], G Hilscher[2], H Michor[2], Ch Paul[2], P Rogl[1,5], A Daoud-Aladine[3], L Keller[3], T Roisnel[4] and H Noel[4]

[1] Institut für Physikalische Chemie, Universität Wien, A-1090 Wien, Währingerstraße 42, Austria
[2] Institut für Festkörperphysik, TU Wien, A-1040 Wien, Wiedner Hauptstraße 8-10, Austria
[3] Laboratorium für Neutronenstreuung, PSI & ETH, CH-5232 Villigen PSI, Switzerland
[4] Laboratoire de Chemie du Solide et Inorganique Moléculaire, Université de Rennes I, UMR CNRS 6511, Avenue du Général Leclerc, F-35042 Rennes cedex, France

E-mail: peter.franz.rogl@univie.ac.at

Received 20 January 2003, in final form 17 March 2003
Published 6 May 2003
Online at stacks.iop.org/JPhysCM/15/3053

Abstract

A novel ternary structure type has been determined from single crystals of $Ce_2Zn_6Ge_3$ grown from indium–zinc flux solvent. The $Ce_2Zn_6Ge_3$ type is hexagonal ($a = 0.767\,69(2)$ nm; $c = 0.411\,59(2)$ nm) with space group $P\bar{6}2m$, $Z = 1$. Isotypic compounds with La, Pr, Nd, Sm and Gd were synthesized by reaction sintering, and their isotypic crystal structures were confirmed from Rietveld refinements. These novel ternaries show metallic behaviour and their ground state depends on the particular rare earth ion. Long-range magnetic order was deduced for the compounds from Ce to Gd, with a maximum transition temperature $T_N \sim 29$ K for $Gd_2Zn_6Ge_3$. While the compounds with Ce and Pr exhibit a spontaneous magnetic type of order, those with Nd, Sm and Gd are antiferromagnetic. The magnetic structures of $Pr_2Zn_6Ge_3$ and $Nd_2Zn_6Ge_3$ were resolved on the basis of neutron powder diffraction performed at 1.5 K.

1. Introduction

Our general interest in crystal structures and physical properties of cerium–, europium– and ytterbium–zinc silicides and germanides [1, 2] prompted us towards a closer inspection of the ternary systems formed by Zn and Ge with rare earth (RE) elements. In particular, compounds with high Si, Ge content may show interesting thermoelectric properties. Due to the low melting and boiling points of zinc metal ($T_m = 419.6\,^\circ$C, $T_b = 907\,^\circ$C [3]), synthesis of zinc

* Dedicated to Professor O Bodak on the occasion of her 60th birthday.
[5] Author to whom any correspondence should be addressed.

containing single-phase materials is difficult to achieve via the usual high-frequency or arc melting techniques. Therefore, there is hitherto rather limited information on the crystal chemistry and properties of ternary RE zinc germanides, for which only a few structure types have been elucidated, such as $RE_4Zn_5Ge_6$ ({RE: Gd, Tm, Lu}) [4], $NdZn_{1.5}Ge_{0.5}$ [5], $YbZn_2Ge_2$ [1], $EuZn_2Ge_2$ [2, 6] and EuZnGe [7]. Phase equilibria within an isothermal section at 600 °C have so far been reported for the ternary systems {Ce, Nd, Gd}–Zn–Ge, revealing a series of ternary compounds; the crystal structures of most of them still remain unknown [8–10].

In recent papers [1, 2, 11, 12], the use of an alternative technique for the growth of sizeable single-crystal material based on the Lebeau method [13] has been demonstrated, employing low-melting flux solvents such as tin, lead, aluminium or copper. This technique has been quite successful in producing transition metal borides as well as silicides and germanides [14–16].

2. Experimental details

Starting materials used were zinc granules, p.A., indium ingots, 99.9% pure, 99.9% pure ingots of RE and Ge pieces, 99.999%. Single crystals of $Ce_2Zn_6Ge_3$ were grown from 60In–40Zn (at.%) flux taken in a mass ratio of 12:1 with an elemental mixture of 33.3Ce–66.7Ge (at.%). Pieces of elements were contained in Al_2O_3 crucibles and vacuum sealed within thick-walled quartz tubes. A typical experiment started from room temperature with a heating rate of 75 °C h^{-1} up to 1100 °C with an intermediate hold for 1 h at a temperature of 450 °C, well above the melting point of the flux. After a soaking period for 24 h, cooling to 500 °C proceeded at a speed of 25 °C h^{-1}, after which the sample batches were kept at this temperature for 12 h prior to final quenching, when samples were simply removed from the hot furnace. The indium–zinc flux was finally dissolved in an ultrasonically agitated bath of mercury at room temperature.

Attempts to grow single crystals of isotypic silicides were unsuccessful: the resulting product contained only single crystals of $CeSi_2$ with $ThSi_2$ structure. It is important to note that pure Zn flux, which was successfully used to grow ternary europium and ytterbium–zinc silicides and germanides [1, 2], did not result in the production of $Ce_2Zn_6Ge_3$. This fact may be explained by a low stability of this compound against dilute HCl used to dissolve the Zn flux.

Taking into account the high vapour pressure of Zn, $Ce_2Zn_6Ge_3$ and isotypic compounds with La, Pr, Nd, Sm and Gd were produced applying the following method. Arc-melted master alloys with nominal composition RE_2Ge_3 (RE: La, Ce, Pr, Nd, Sm, Gd) were powdered under cyclohexane and mixed with freshly prepared Zn powder. The compacted powder blends were sealed in evacuated silica ampoules and heat treated at 350–400 °C for 4–7 days, after which a fine powder of nearly single-phase $RE_2Zn_6Ge_3$ was obtained. It was re-compacted and sintered again to obtain a single-phase material usable for physical property measurements. Contents of secondary phases (typically Zn and/or Ge) were examined by quantitative x-ray powder Rietveld refinement and found not to exceed 3–5 vol.%. Attempts to produce isotypic compounds with europium and ytterbium failed; they merely resulted in the formation of $EuZn_2Ge_2$ and $YbZn_2Ge_2$, previously described in [1, 2].

X-ray examination of polycrystalline materials was performed at room temperature in a Guinier–Huber x-ray camera with an Image Plate recording system (Cu Kα_1) employing an internal standard of 99.9999 mass% pure Si (a_{Si} = 0.543 1065 nm). Neutron diffraction was carried out on the DMC spectrometer of the PSI spallation source SINQ with $\lambda_{neutron}$ = 0.255 924 nm. Quantitative Rietveld refinement of single-phase samples was performed by means of the FULLPROF program [17]. A series of crystal specimens

was inspected using a 57.3 mm radius Gandolfi camera, which also served for preliminary determination of the unit-cell dimensions. Weissenberg photographs accomplished crystal quality control and determination of crystal symmetry. Single-crystal x-ray intensity data for $Ce_2Zn_6Ge_3$ were collected for a hemisphere in 271 images on a four-circle Nonius Kappa diffractometer equipped with a CCD area detector (graphite monochromatic Mo Kα radiation, $\lambda = 0.071\,073$ nm). Orientation matrix and unit-cell parameters for a hexagonal crystal system ($a = 0.767\,69(2)$ and $c = 0.411\,59(2)$ nm) were derived using the program DENZO [18]). Absorption correction was taken from the program SORTAV [18] ($\mu_{Ce_2Zn_6Ge_3} = 37.8$ mm^{-1}) and the structure was refined with the aid of the SHELXS-97 program [19].

Measurements of the various bulk properties were carried out with a series of standard techniques; details are given in [20].

3. Results and discussions

3.1. Structural chemistry

3.1.1. Crystal structure of $Ce_2Zn_6Ge_3$. As the absence of systematic extinctions in $Ce_2Zn_6Ge_3$ is compatible with several hexagonal (and trigonal) space groups, determination of the atom arrangement was successful in the low-symmetry space group $P\bar{3}$ employing direct methods with the program SIR. Search for higher symmetry (program MISSYM) prompted the highest possible symmetry in space group $P\bar{6}2m$. With respect to the known difficulties in distinguishing Zn and Ge atoms by x-ray methods, balanced thermal displacement factors and interatomic distances in agreement with the sum of the metal radii were used to locate Ge atoms, which were found to occupy the 3g site $(0.3808, 0, 1/2)$. Thus a fully ordered atom arrangement is obtained for a formula $Ce_2Zn_6Ge_3$ in good agreement with fairly single-phase bulk samples prepared from the elements, and with composition controlled by EPMA. Consistency also exists for the lattice parameters of bulk alloys and the single-crystal specimens, ruling out any contamination or solubility of In flux in the single crystals. Occupancies of all crystallographic sites were refined but did not reveal any significant deviations from stoichiometry. Refining anisotropic thermal displacement factors in the final run yielded an R-value as low as 0.03, confirming the structure model. Results of the structure determination are listed in table 1; the structure of $Ce_2Zn_6Ge_3$ is presented in figure 1(a) in a three-dimensional view along the [001]-axis.

As one of the typical structural units for RE germanides, $REGe_x$, Ge atoms form trigonal prisms around the RE atoms. The next-nearest-neighbour coordination around the Ce atoms is increased by three additional Zn1 atoms around the waist of the triangular prism. Six more Zn2 atoms enlarge the coordination figure around Ce to CN = 15 (9 nearest + 6 second-nearest neighbours) in the form of a slightly distorted hexagonal prism with each second wall face centred by a Zn1 atom. Zinc atoms form $[Zn_9]$ clusters face connected in the form of an infinite column parallel to [001]. These columns are framed in channels constructed from six edge-connected $Ce[Ge_6]$ triangular prisms stacked along [001]. Such a type of channel is common to Fe_2P(ZrNiAl)-type structures, but in Fe_2P the centre column simply consists of a row of triangular prisms. The centre of the $[Zn_9]$ cluster in $Ce_2Zn_6Ge_3$ at $0, 0, 1/2$ provides space for a small tetrakaidecahedrally coordinated void, which may be filled by atoms with radii of about 0.1 nm. However, no residual electronic density in this site was established by difference Fourier analysis. Interatomic distances (see table 1) agree well with the metallic radii of pure elements except for the Zn1–Zn1 bond length, which shows a reduction of about 5%.

The architecture of the $Ce_2Zn_6Ge_3$ structure shows a number of features related to the well known AlB_2 type. This can be seen from a projection of the structure on the xy-plane (figure 1(b)). Ge and Zn2 atoms form distorted hexagonal prisms around Ce atoms, which in

Table 1. Structural data[(a)] of $RE_2Zn_6Ge_3$ (RE = La, Ce, Pr, Nd, Sm, Gd) (space group $P\bar{6}2m$, No 189).

Parameter	$La_2Zn_6Ge_3$	$Ce_2Zn_6Ge_3$	$Pr_2Zn_6Ge_3$	$Nd_2Zn_6Ge_3$	$Sm_2Zn_6Ge_3$	$Gd_2Zn_6Ge_3$
a (nm)	0.770 88(2)	0.767 69(2)	0.765 43(2)	0.763 78(2)	0.761 19(2)	0.759 39(3)
c (nm)	0.414 96(3)	0.411 59(2)	0.409 84(3)	0.408 17(3)	0.405 19(1)	0.402 95(3)
Data collection	Image Plate	Nonius Kappa CCD	Image Plate	Image Plate	Image Plate	Image Plate
Radiation	Cu Kα	Mo Kα	Cu Kα	Cu Kα	Cu Kα	Cu Kα
Reflections measured	63	678 > $4\sigma(F_0)$ of 698	63	63	61	60
Θ range	$12.5 \leqslant 2\Theta \leqslant 100$	$2.04 \leqslant 2\Theta \leqslant 90.58$	$12.5 \leqslant 2\Theta \leqslant 100$	$12.5 \leqslant 2\Theta \leqslant 100$	$12.5 \leqslant 2\Theta \leqslant 100$	$12.5 \leqslant 2\Theta \leqslant 100$
Number of variables	26	16	26	26	26	26
$R_F = \Sigma\|F_o - F_c\|/\Sigma F_o$	0.050	$R_{F2}(678) = 0.033$	0.057	0.030	0.050	0.056
$R_I = \Sigma\|I_{oB} - I_{cB}\|/\Sigma I_{oB}$	0.051	$R_{F2}(698) = 0.034$	0.050	0.036	0.050	0.054
$R_{wP} = [\Sigma w_i\|y_{oi} - y_{ci}\|^2/\Sigma w_i\|y_{oi}\|^2]^{\frac{1}{2}}$	0.072	$wR2 = 0.080$; $R_{int} = 0.541$	0.069	0.042	0.032	0.023
$R_P = \Sigma\|y_{oi} - y_{ci}\|/\Sigma\|y_{oi}\|$	0.049	Mosaicity = 0.565(3)	0.048	0.029	0.023	0.017
$R_e = [(N - P + C)/\Sigma w_i y_{oi}^2)]^{\frac{1}{2}}$	0.025	Extinction = 0.130(7)	0.021	0.008	0.019	0.016
$\chi^2 = (R_{wP}/R_e)^2$	8.3	GOF = 1.074	11.0	22.7	2.84	1.98
		Atom parameters				
RE: in 2c (1/3, 2/3, 0)	La	Ce	Pr	Nd	Sm	Gd
B_{iso}(10^2 nm^2)	0.38(2)	$U_{equ.} = 0.0069(1)$[a]	0.46(2)	0.62(2)	0.63(1)	1.06(2)
Zn1: in 3f (x, 0, 0)	$x = 0.1880(2)$	$x = 0.1896(1)$	$x = 0.1888(2)$	$x = 0.1897(1)$	$x = 0.1909(1)$	$x = 0.1916(1)$
B_{iso}(10^2 nm^2)	0.67(4)	$U_{equ.} = 0.0107(2)$[a]	0.86(5)	0.89(3)	0.73(3)	0.57(3)
Zn2: in 3g (x, 0, 1/2)	$x = 0.7089(2)$	$x = 0.7107(1)$	$x = 0.7096(2)$	$x = 0.7112(1)$	$x = 0.7132(1)$	$x = 0.7128(1)$
B_{iso}(10^2 nm^2)	0.71(4)	$U_{equ.} = 0.0127(2)$[a]	0.75(4)	0.75(3)	0.55(3)	0.55(3)
Ge: in 3g (x, 0, 1/2)	$x = 0.3775(2)$	$x = 0.3808(1)$	$x = 0.3810(2)$	$x = 0.3827(1)$	$x = 0.3860(1)$	$x = 0.3871(1)$
B_{iso}(10^2 nm^2)	0.57(4)	$U_{equ.} = 0.0075(1)$[a]	0.62(4)	0.67(2)	0.53(2)	0.70(2)

Table 1. (Continued.)

Parameter	$La_2Zn_6Ge_3$	$Ce_2Zn_6Ge_3$	$Pr_2Zn_6Ge_3$	$Nd_2Zn_6Ge_3$	$Sm_2Zn_6Ge_3$	$Gd_2Zn_6Ge_3$
	Interatomic distances (nm); standard deviations generally <0.0005 nm					
RE–6Ge	0.318 56	0.315 97	0.314 82	0.313 51	0.311 22	0.309 83
RE–3Zn1	0.327 66	0.325 41	0.324 90	0.323 70	0.321 93	0.320 78
RE–6Zn2	0.344 23	0.342 97	0.341 39	0.341 00	0.340 09	0.338 76
Zn1–2Zn1	0.251 01	0.252 10	0.250 30	0.250 95	0.251 68	0.252 01
Zn1-2Zn2	0.286 15	0.283 78	0.283 13	0.281 67	0.279 45	0.278 56
Zn1–Ge	0.253 74	0.252 77	0.252 26	0.251 75	0.251 19	0.250 26
Zn2–Ge	0.264 08	0.253 26	0.251 52	0.250 90	0.249 06	0.247 33

[a] Crystal structure data were standardized using the program Structure Tidy [27].
[b] Anisotropic atomic displacement parameters (10^2 nm^2): Ce: $U_{11} = U_{22} = 0.006(1)$, $U_{33} = 0.0074(1)$, $U_{12} = 0.00330(6)$; Zn1: $U_{11} = 0.0091(2)$; $U_{22} = 0.0142(4)$, $U_{33} = 0.0105(3)$, $U_{12} = 0.0071(2)$; Zn2: $U_{11} = 0.0095(3)$, $U_{22} = 0.0086(4)$, $U_{33} = 0.0197(4)$, $U_{12} = 0.0127(2)$; Ge: $U_{11} = 0.0070(2)$; $U_{22} = 0.0079(3)$, $U_{33} = 0.0080(2)$, $U_{12} = 0.0039(1)$.

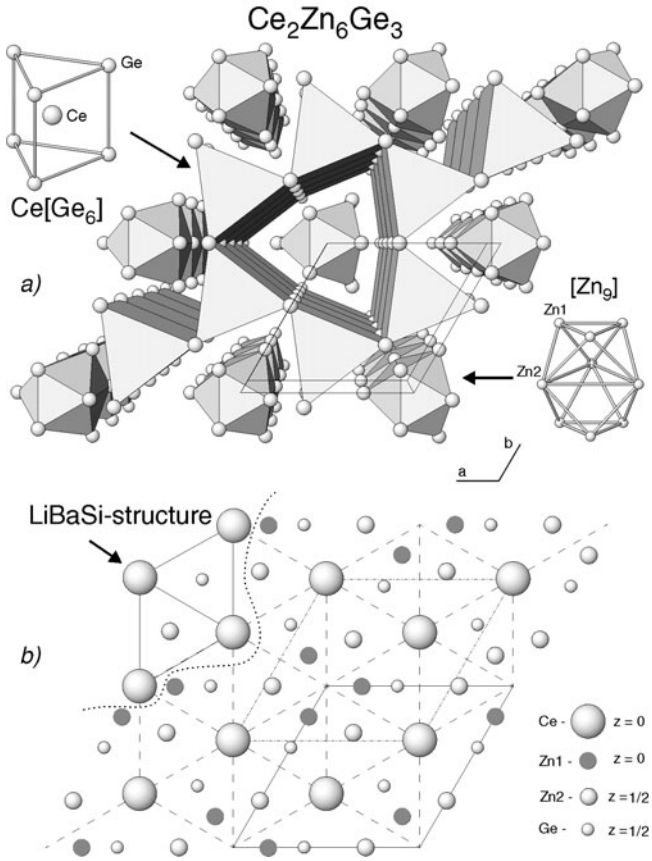

Figure 1. Crystal structure of $Ce_2Zn_6Ge_3$: three-dimensional presentation (a) and projection on xy-plane (b). Two different unit cells are outlined: the standardized unit cell (see table 1) is given by a solid line; the magnetic unit cell is represented by a dashed–dotted line (see figure 3). The dotted curve separates the $Ce_2Zn_6Ge_3$ structure from the related LiBaSi-type cell.

turn comply with a regular hexagonal pattern (dashed lines in figure 1(b)), resembling Al atoms in AlB_2. As a major difference, site $1a(0, 0, 0)$ is unoccupied in $Ce_2Zn_6Ge_3$ but is surrounded by three Zn1 atoms. Simple substitution of three Zn1 atoms (in 3f positions) by one large Ce atom at $1a$ transforms the $Ce_2Zn_6Ge_3$ structure into the AlB_2 type (LiBaSi-ordered variant). The transformation prompts a slight displacement of Zn2 and Ge atoms into the centres of the trigonal prisms formed by Ce atoms. Consequently, the replacement results in a hypothetical compound with AlB_2 structure: $Ce_2(Zn_3)Zn_3Ge_3 \equiv Ce_2(Ce)Zn_3Ge_3 \equiv CeZnGe$ (claiming a smaller unit cell $a_0 = a/\sqrt{3}$; see figure 1(b)).

3.1.2. Isotypic compounds $RE_2Zn_6Ge_3$, $RE = La, Pr, Nd, Sm, Gd$. Indexing of the x-ray powder patterns of $RE_2Zn_6Ge_3$ alloys for RE = La, Pr, Nd, Sm, Gd in all cases prompted a hexagonal unit cell close to that established for $Ce_2Zn_6Ge_3$. Analysis of the x-ray intensities, absence of systematic extinctions, and size of unit cells suggest isotypism with the structure type of $Ce_2Zn_6Ge_3$. Rietveld refinements confirmed the isotypism; results are compiled in table 1. The small and rather insignificant variation in the lattice parameters (figure 2) indicates the absence of homogeneity regions. The graph, volume versus RE, clearly reveals a 3+ ground state for Ce and Sm.

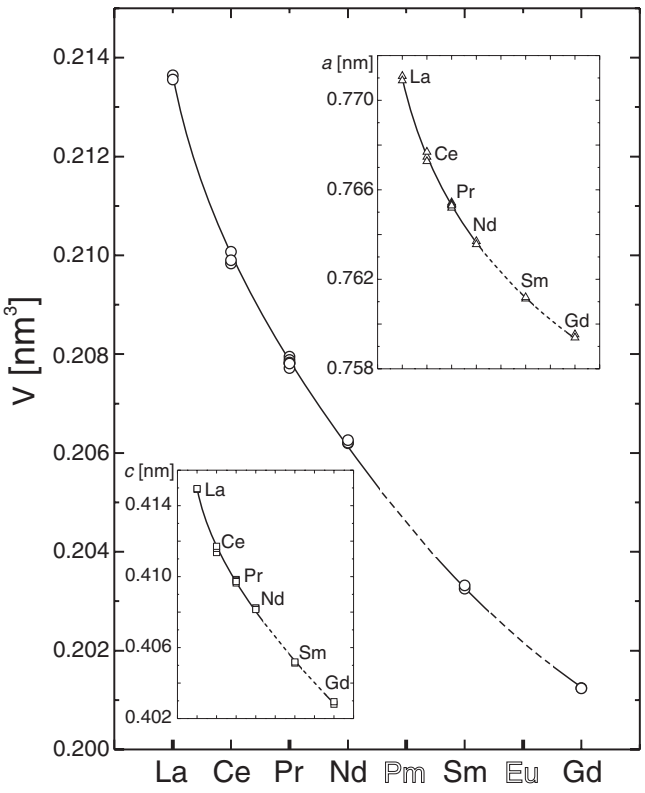

Figure 2. Lattice parameters and unit-cell volume of $RE_2Zn_6Ge_3$ versus RE.

From the results obtained, one could assume that the new compound $Nd_2Zn_6Ge_3$ may participate in the phase equilibria determined for the 600 °C isothermal section Nd–Zn–Ge [8], for which several compounds with unknown structure type were listed. However, neither a compound '$Nd_2Zn_{15}Ge_2$' nor '$NdZn_2Ge$' corresponds to our formula $Nd_2Zn_6Ge_3$. To establish stability of $Nd_2Zn_6Ge_3$ at higher temperature this specimen was re-annealed at 600 °C for 2 weeks. X-ray inspection of the annealed sample again revealed single-phase $Nd_2Zn_6Ge_3$ with lattice parameters ($a = 0.763\,90(2)$ nm and $c = 0.408\,18(2)$ nm) close to those observed at 400 °C (see table 1).

3.1.3. Magnetic structure of $Nd_2Zn_6Ge_3$ and $Pr_2Zn_6Ge_3$. Analysis of neutron diffraction patterns of $Pr_2Zn_6Ge_3$ at 9 K and $Nd_2Zn_6Ge_3$ at 7 K confirmed the x-ray data; in particular, the difference in the neutron scattering length of Zn and Ge allowed unambiguous atom site distribution. Neutron data at lower temperatures (5.5 and 4 K, respectively) revealed additional reflections of magnetic origin. The magnetic unit cells in both cases were indexed on the basis of the hexagonal parent structure with the a-parameter identical to that of the nuclear cell, but with a multiple c-parameter: for $Pr_2Zn_6Ge_3$ $c_{mag} = 3c_{nuc}$ and for $Nd_2Zn_6Ge_3$ $c_{mag} = 2c_{nuc}$. The magnetic structures of $Pr_2Zn_6Ge_3$ and $Nd_2Zn_6Ge_3$ at 1.5 K were resolved as co-linear antiferromagnets, with ordered magnetic moments of 2.97(7) μ_B and 2.20(4) μ_B for Pr and Nd, respectively. As one can see from figure 3(a), the magnetic structure of $Pr_2Zn_6Ge_3$ is an antiferromagnetic alternation of $++-++-++-\cdots$ ferromagnetic (a, b) planes of Pr atoms with moments along the c-axis. The magnetic structure of $Nd_2Zn_6Ge_3$ (figure 3(b)) is formed

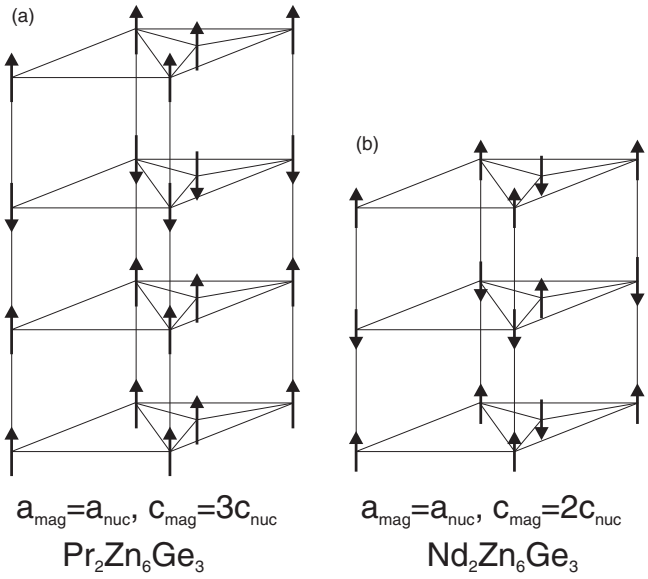

Figure 3. Magnetic structures of $Pr_2Zn_6Ge_3$ (a) and $Nd_2Zn_6Ge_3$ (b) based on the unit cell outlined in figure 1(b) by a dashed–dotted line.

by antiferromagnetic (a, b) planes which are stacked antiferromagnetically along the c-axis. In both refinements magnetic R-factors are below 9%.

3.2. Physical properties

Temperature dependent magnetic phenomena and transport properties were studied for the ternary RE compounds described above in order to characterize the respective ground states and to figure out phase transitions appearing in this series. Moreover, thermoelectric performance was determined.

Figure 4(a) shows the temperature dependent magnetic susceptibility χ plotted as χ^{-1} versus T for $RE_2Zn_6Ge_3$, where RE are the light rare earths. Common to all the investigated compounds is a Curie–Weiss-like behaviour at elevated and anomalies at lower temperatures, indicating magnetic phase transitions (compare figure 4(b)). To qualitatively account for the region above about 50 K, least-squares fits according to the modified Curie–Weiss law, i.e., $\chi = \chi_0 + C/(T - \theta_p)$, were applied. χ_0 represents a temperature independent Pauli-like susceptibility, C is the Curie constant and θ_p is the paramagnetic Curie temperature. Results of this procedure are summarized in table 2. Effective magnetic moments of this series are very near to the theoretical values associated with the 3+ state of the particular RE ion. Slightly larger deviations occur for $Ce_2Zn_6Ge_3$ with $\mu_{eff} = 2.32\,\mu_B$ compared to Ce^{3+} with $\mu_{eff} = 2.54\,\mu_B$. Such a difference may follow from some hybridization of the $4f^1$ state of Ce with the conduction band resulting in deviations from the 3+ integer valence state. Alternatively, one may consider crystal electric field (CEF) splitting with the uppermost level situated well above the ground state. To estimate the influence of crystal field splitting, we used the Van Vleck formula to account for the magnetic susceptibility in the presence of a CEF with hexagonal symmetry. Additionally, one has to consider molecular field contributions, i.e.

$$\frac{1}{\chi} = \frac{1}{\chi_{CEF}} - \eta \tag{1}$$

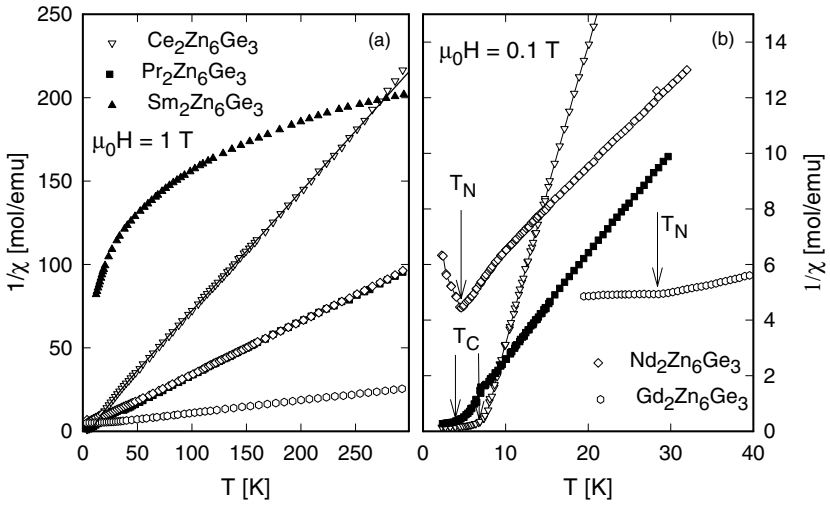

Figure 4. (a) Temperature dependent susceptibility χ of $RE_2Zn_6Ge_3$ plotted as χ^{-1} versus T; $\mu_0 H = 1$ T. The solid curve is a least-squares fit (for details see the text). Data for $Sm_2Zn_6Ge_3$ are divided by a factor of three. (b) Low-temperature features of χ^{-1} versus T of $RE_2Zn_6Ge_3$; $\mu_0\ H = 0.1$ T.

Table 2. Magnetic data[a] of $RE_2Zn_6Ge_3$ (RE = Ce, Pr, Nd, Sm and Gd).

	Ordering temperature (K)	Effective magnetic moment (μ_B)	Paramagnetic Curie temperature (K)	Magnetization at 2 K and 6 T (μ_B/fu)
$Ce_2Zn_6Ge_3$	7.2	2.32	0.6	1.58
$Pr_2Zn_6Ge_3$	7.1	3.4	1.1	2.7
$Nd_2Zn_6Ge_3$	4.6	3.55	−6.8	1.56
$Sm_2Zn_6Ge_3$	7.3	0.58	−23	—
$Gd_2Zn_6Ge_3$	28.8	7.08	−40	2.2

[a] Standard deviations: for measured temperatures smaller than 0.1 K; for deduced temperatures smaller than 1 K; for effective magnetic moments smaller than 0.05 μ_B; for magnetization smaller than 0.02 μ_B.

where χ_{CEF} is due to crystal field effects and η is the molecular field parameter. Since the analysis is based completely on data obtained on polycrystalline samples, χ_{CEF} should be given by

$$\chi_{CEF} = \tfrac{1}{3}\chi_{\parallel} + \tfrac{2}{3}\chi_{\perp}, \tag{2}$$

where $\chi_{\parallel}$ and $\chi_{\perp}$ are the components parallel and perpendicular to the c-axis, respectively. Employing the particular expression derived by Mader and Swift for $J = 5/2$ and hexagonal symmetry [21] allows us to roughly determine the CEF scheme. A least-squares fit to $\chi(T)$ of $Ce_2Zn_6Ge_3$ reveals the doublet Γ_7 as the ground state followed by Γ_9 about 140 K above and the uppermost level Γ_8 about 400 K above the ground state. Such a significant separation may, most likely, explain the slightly reduced effective magnetic moment of the cerium ion, deduced from measurements below room temperature. However, one should keep in mind that this CEF scheme is just of preliminary nature due to the usage of polycrystalline material and has to be corroborated by inelastic neutron scattering experiments. The molecular field constants $\eta_{\parallel}$ and $\eta_{\perp}$ are 4.7 and 14 emu mol^{-1}, respectively, indicating ferromagnetic interactions.

It is interesting to note that the paramagnetic Curie temperature θ_p is found to be positive in the case of the Ce and the Pr based compounds, while θ_p is negative for Nd, Sm and Gd (table 2). In general, the sign of θ_p characterizes the type of interaction between the magnetic moments of the RE ions. While positive values reflect ferromagnetic interactions, negative values are a signature of antiferromagnetic interactions. Experimental results thus should evidence a crossover from ferro- to antiferromagnetism. In fact, isothermal magnetization measurements (figure 5) taken at 2 K evidence substantial changes when proceeding through the series. Starting with $Ce_2Zn_6Ge_3$, spontaneous magnetization is found and a value of about 1.6 μ_B is obtained at 6 T. The individual contribution of each Ce ion would then be 0.8 μ_B. With respect to the saturation magnetization associated with the Ce^{3+} ion ($M_{sat} = g_j J = 2.14\ \mu_B$), the observed value appears to be rather small, a finding that has to be attributed to the lifting of the ground state degeneracy ($N = 2J + 1$) by CEF effects. Moreover, the rather field independent $M(H)$ curve at 2 K indicates that the first excited level is well separated from the ground state doublet, backing the conclusions drawn from susceptibility data. Although the spin structure of $Pr_2Zn_6Ge_3$ is antiferromagnetic (see figure 3), net magnetization is expected and in fact found from the isothermal magnetization measurements at 2 K. But at a field slightly above 1 T, a field induced change occurs, possibly aligning further Pr moments along the *c*-axis. Above this spin reorientation, only a slight increase of the magnetization is found up to 6 T, although the magnetization at 6 T is still below the full value of 5.94 μ_B/fu expected from neutron data. Differences between the magnetic moment deduced from neutron data ($\mu = 2.97\ \mu_B$/Pr atom) and the corresponding value obtained from the isothermal magnetization curve are caused by the fact that polycrystalline material was used and hence only a fraction (in general about one-third, since magnetic moments are parallel to the *c*-direction) will contribute to the measured bulk effect. Moreover, the saturation value associated with the magnetic structure presented in figure 3 cannot be derived because an external field of 1 T triggers a spin reorientation. A rough estimation compares the magnetization of 0.5 μ_B/Pr atom, as measured at 2 K and 1 T (just below the spin reorientation), with the value of about 0.7 μ_B/Pr atom, as derived from the neutron data: here the resulting 5.94 μ_B per magnetic unit cell corresponds to 1.97 μ_B per crystallographic unit cell, and when taking into account the factor of one-third correcting for the uniaxial spin alignment in a polycrystalline material we arrive at 0.7 μ_B/Pr atom. $Nd_2Zn_6Ge_3$, $Sm_2Zn_6Ge_3$ and $Gd_2Zn_6Ge_3$ do not exhibit spontaneous magnetization, thus some type of antiferromagnetic ground state should be present as verified for $Nd_2Zn_6Ge_3$ from neutron diffraction (type I antiferromagnet). Metamagnetic transitions as a further hint to antiferromagnetism occur around 3 T for Nd and 5.5 T for Gd, respectively.

Figure 6 displays the temperature dependent specific heat (left-hand scale) and the magnetic entropy (right-hand scale) of two members of $RE_2Zn_6Ge_3$. Non-magnetic $La_2Zn_6Ge_3$ exhibits at low temperature a smooth increase; a standard plot C_p/T versus T^2 below 8 K reveals a Sommerfeld value $\gamma = 2$ mJ mol K^{-2} and $\beta = 0.001\,02$ J mol^{-1} K^{-4}. This allows us to determine the Debye temperature as $\Theta_D^{LT} = 275$ K. The application of the simple Debye model in the whole temperature range up to 100 K, however, does not reveal convincing fits. In order to derive more accurate information about the lattice dynamics of this family of compounds, we have not only used a Debye spectrum, rather, Einstein frequencies are added. The model thus employed can be written as

$$C_{ph}(T) = \frac{9R}{\omega_D^3}\int_0^{\omega_D} \frac{\omega^2(\frac{\omega}{2T})^2}{\sinh^2(\frac{\omega}{2T})}\,\mathrm{d}\omega + \sum_{i=1,2,3} c_i R \frac{(\frac{\omega_{Ei}}{2T})^2}{\sinh^2(\frac{\omega_{Ei}}{2T})}. \tag{3}$$

The first part of equation (3) represents the Debye contribution and the second part accounts for three additional Einstein frequencies with weights $c_1 = 20$, $c_2 = 5$ and $c_3 = 5$. A least-

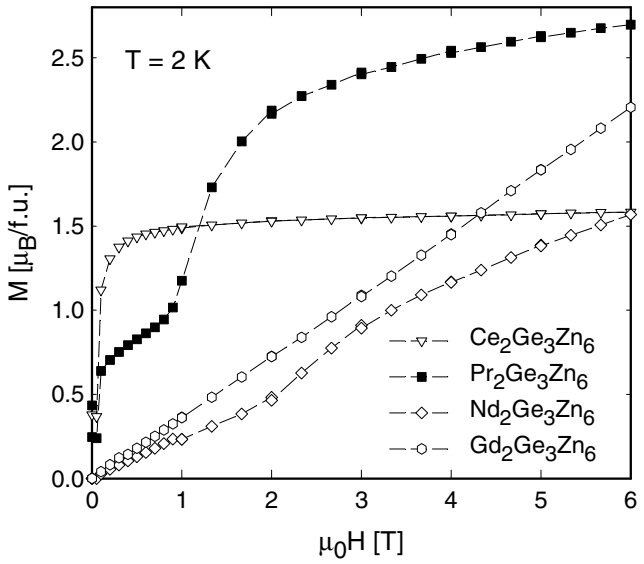

Figure 5. Isothermal magnetization M of $RE_2Zn_6Ge_3$ plotted as M versus μ.

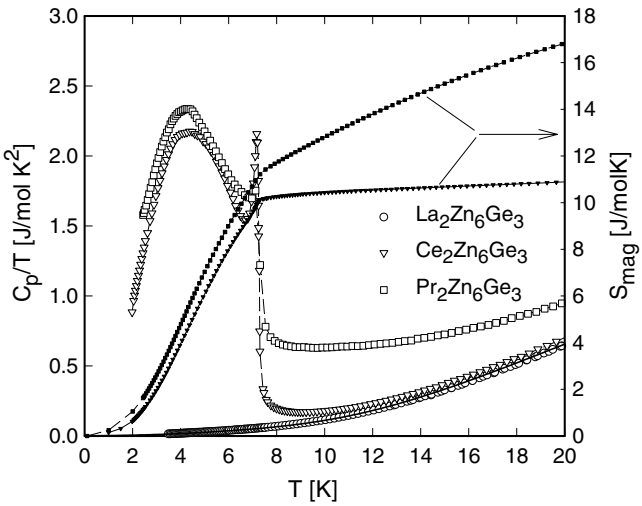

Figure 6. Left-hand scale: temperature dependent specific heat of $RE_2Zn_6Ge_3$, RE = La, Ce, Pr. The solid curve is a least-squares fit (for details see the text). Right-hand scale: temperature dependent magnetic entropy of $Ce_2Zn_6Ge_3$ and $Pr_2Zn_6Ge_3$.

squares fit of equation (3) to the experimental data (solid curve, figure 6) reveals excellent agreement with $\Theta_D = 125$ K, $\omega_{E1} = 193$ K, $\omega_{E2} = 105$ K and $\omega_{E3} = 350$ K.

Magnetic $Ce_2Zn_6Ge_3$ and $Pr_2Zn_6Ge_3$ are characterized by pronounced anomalies around 7 K, marking the onset of long-range magnetic order. The height of the jump at $T = T_{ord}$ evidences bulk properties and excludes impurities from being responsible for the phase transition observed. The magnetic entropies S_{mag} of $Ce_2Zn_6Ge_3$ and $Pr_2Zn_6Ge_3$ are plotted in figure 6 as filled, small symbols on the right-hand scale. At T_{ord}, S_{mag} reaches 10.2 and 11.2 J mol^{-1} K^{-1} per formula unit, respectively, which is roughly twice $R \ln 2$, expected for

ordering of two magnetic ions per formula unit in a doublet ground state. CEF originating from charges in hexagonal symmetry causes a lifting of the ground state degeneracy of the total angular momentum of Ce ($J = 5/2$) and Pr ($J = 4$) and results in Schottky contributions to the specific heat at higher temperatures. As obvious from the observed entropies, there might be a significant difference in level splitting between both compounds. While the former (Ce) shows only a slight increase of $S_{mag}(T)$ in the paramagnetic temperature range, the latter (Pr) reaches $2 \times R \ln 4$ at about 60. This indicates that CEF splitting creates a large separation of the first excited level from the ground state in the case of Ce, but a substantially smaller one for the Pr based compound. With respect to $Ce_2Zn_6Ge_3$ this observation nicely matches the findings derived from the magnetic data.

In order to explore the thermoelectric performance of the present family of compounds, we have studied the temperature dependent electrical resistivity as well as thermopower and thermal conductivity. The former also allows us to accurately account for phase transitions in these materials as well. Plotted in figure 7 is the temperature dependent resistivity $\rho(T)$ of $RE_2Zn_6Ge_3$ with RE = La, Ce, Pr, Nd, Sm and Gd. Since the investigated materials were produced in sintered form, we normalized the data to their respective room-temperature values. To disambiguate the graph, the $\rho(T)$ curve of $La_2Zn_6Ge_3$ is shifted by a value of 0.1. Low-temperature features in $\rho(T)$ are shown in the inset of figure 7. $La_2Zn_6Ge_3$ does not carry permanent magnetic moments, therefore $\rho(T)$ should behave like that of a simple metal following a temperature dependence according to the Bloch–Grüneisen law, i.e.,

$$\rho(T) = \rho_0 + 4R\Theta_D\left(\frac{T}{\Theta_D}\right)^5 \int_0^{\Theta_D/T} \frac{x^5\,\mathrm{d}x}{(\mathrm{e}^x - 1)(1 - \mathrm{e}^{-x})}. \tag{4}$$

Here, ρ_0 is the residual resistivity, R is the temperature independent electron–phonon interaction constant and Θ_D is again the Debye temperature. A closer inspection of the data, however, evidences a rather strong curvature, which usually requires the addition of an extra term KT^3, known as the Mott–Jones contribution [22]. The origin of this term is usually a narrow band in the vicinity of the Fermi energy. A least-squares fit to $\rho(T)$ of $La_2Zn_6Ge_3$ then reveals a Debye temperature of about 175 K. All the other compounds of this series are characterized by a pronounced kink at lower temperatures marking the onset of long-range magnetic order. The absolute values of the transition temperatures are in fine agreement with the values deduced from susceptibility measurements. Besides the phonon and the residual contribution, the resistivity in the paramagnetic region also consists of a spin-disorder part ρ_{spd}, which in the absence of crystal field splitting is expected to be temperature independent [23]. In the case of a Gd ion, the total angular momentum is just composed of the spin moments; as a consequence, crystal field splitting does not occur and ρ_{spd} should be constant. In fact, $Gd_2Zn_6Ge_3$ shows an almost linear behaviour well above T_N, whereas $\rho(T)$ of the other compounds exhibit characteristic curvatures originating from CEF effects, lifting the ground state degeneracies associated with the respective total angular momenta of the light RE ions.

Frequently, cerium compounds are characterized by a pronounced Kondo type of interaction, causing, e.g., a logarithmic contribution to the electrical resistivity and large negative values of the magnetoresistance as well as enhanced values of the Sommerfeld constant of the specific heat. The field response of the resistivity of $Ce_2Zn_6Ge_3$ (figure 8) shows a complicated dependence, being essentially positive for temperatures below T_C, whilst magnetoresistance is negative slightly above T_C and for fields below 8 T. Well above T_C magnetoresistance is positive for all fields applied. As positive magnetoresistance in the magnetically ordered region is usually a fingerprint of antiferromagnetism [24], the isothermal magnetization curve of $Ce_2Zn_6Ge_3$ taken at 2 K, saturating already in fields of about 1 T, can only be conceived in terms of a complicated, possibly non-collinear ferromagnetism. If this

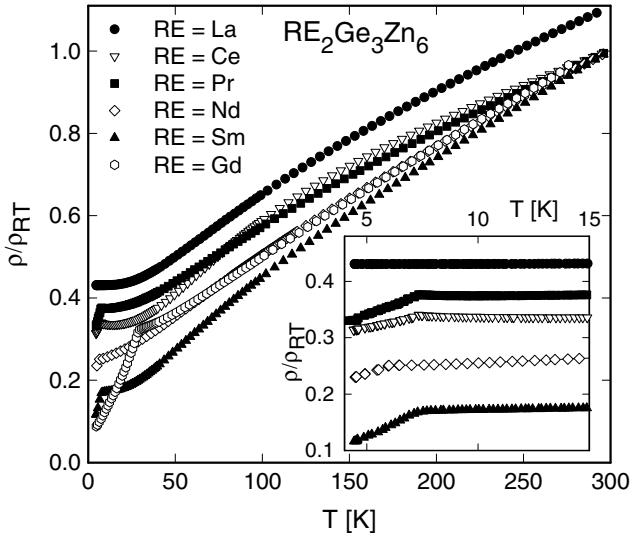

Figure 7. Temperature dependent electrical resistivity ρ of $RE_2Zn_6Ge_3$ plotted as ρ versus T. The inset shows low-temperature features of $RE_2Zn_6Ge_3$. $\rho(T)$ of $La_2Zn_6Ge_3$ is shifted by a value of 0.1.

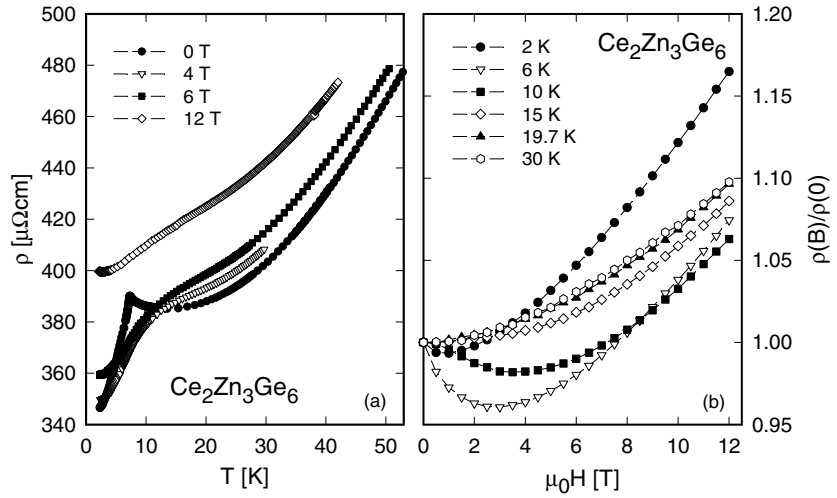

Figure 8. (a) Temperature dependent electrical resistivity ρ of $Ce_2Zn_6Ge_3$ at various applied magnetic fields. (b) Isothermal magnetoresistance $\rho(B)/\rho(0)$ of $Ce_2Zn_6Ge_3$ for various temperatures.

assumption holds, a field induced fully ferromagnetic state is expected to occur for higher fields than available (12 T). Negative magnetoresistance observed in a certain temperature region above T_C complies nicely with quenching of spin fluctuations associated with the magnetic phase transition. At higher temperatures classical (positive) magnetoresistance seems to dominate. The clearly revealed phase transition associated with magnetic ordering is gradually smeared out in increasing magnetic fields (compare figure 8(a)).

The temperature dependent thermopower S is displayed in figure 9(a). Independent of the magnetic state, $S(T)$ is negative throughout the investigated temperature range. Moreover, the

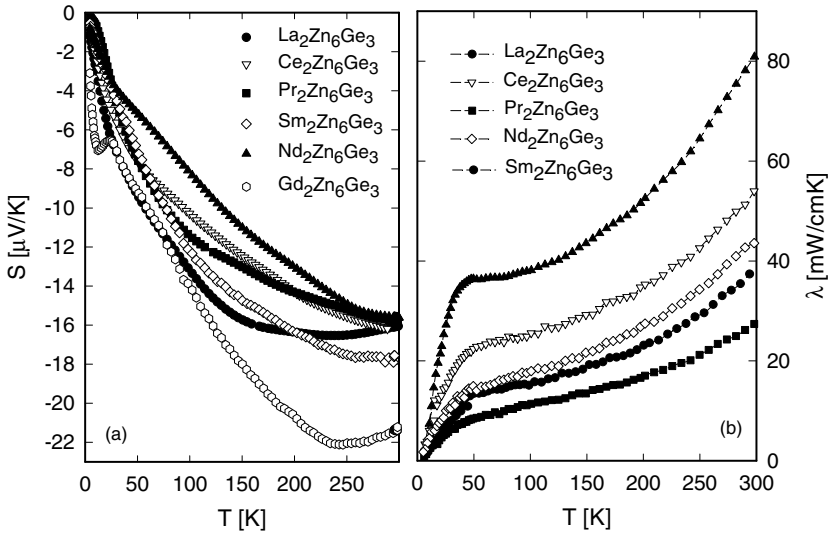

Figure 9. (a) Temperature dependent thermopower S of $RE_2Zn_6Ge_3$. (b) Temperature dependent thermal conductivity λ of $RE_2Zn_6Ge_3$.

absolute values are of comparable magnitude for all compounds studied, reaching -22 μV K^{-1} for $Gd_2Zn_6Ge_3$ at 240 K. The negative values and the fact that $S(T)$ shows little structure up to room temperature indicate that primarily electrons are the charge carriers and interactions between them are small. This also holds for $Ce_2Zn_6Ge_3$. If Kondo interactions are dominating the ground state properties of the latter, large $S(T)$-values could be expected [25] and the appearance of long-range magnetic order at low temperatures would cause a change of the sign of thermopower [26] at temperatures well above the transition temperature. These facts point therefore to a quite normal behaviour of $Ce_2Zn_6Ge_3$ and, thus, the Kondo type of interaction plays only a minor role. The overall $S(T)$-values of the series investigated are too small to be considered for thermoelectric applications. The latter requires, at least, values well above 100 μV K^{-1}.

Thermal conductivity has been measured for all compounds in the temperature range from 4.2 to 300 K (figure 9(b)). Although absolute values seem to be low, thermal conductivity is probably severely influenced by grain boundary effects in the porous sintered pellets. As a consequence, irregularities arise out of line with the expected sequence inferred from an increasing magnetic scattering effect when proceeding from La to Gd. Analysis in terms of the Wiedemann Franz law results in practically equal contributions of phonons and electrons to the total measured thermal conductivity.

4. Summary

Ternary $RE_2Zn_6Ge_3$ compounds with RE = La, Ce, Pr, Nd, Sm and Gd were synthesized using either an indium–zinc flux method or a multi-stage sintering process and found to crystallize in the novel hexagonal $Ce_2Zn_6Ge_3$ structure with space group $P\bar{6}2m$. The physical properties of the present series are characterized by an interesting evolution of the ground state behaviour, documented by a change from ferro-to antiferromagnetism when proceeding from $Ce_2Zn_6Ge_3$ to $Gd_2Zn_6Ge_3$. The magnetic structures of $Pr_2Zn_6Ge_3$ and $Nd_2Zn_6Ge_3$ are simple antiferromagnetic stackings of ferromagnetic (Pr) and antiferromagnetic (Nd) (a, b) planes

with moments aligned along the *c*-axis. The investigations carried out on the Ce-containing compound indicate that the magnetic state is most likely not a simple arrangement of Ce moments; rather, the observed magnetization values as well as magnetoresistance point at a more complicated non-collinear alignment of spins where the projection of the moments yields a net magnetization. Moreover, crystal field splitting (except for Gd), causing a lifting of the ground state degeneracy, is responsible for reduced moments when compared to the respective values of the RE^{3+} ions. The Kondo effect seems not to be the primary interaction mechanism determining the ground state physics of $Ce_2Zn_6Ge_3$. Although the thermal conductivity of these ternaries is rather small due to the complex crystal structure, the absolute values of thermopower do not exceed $-22\ \mu V\ K^{-1}$.

Acknowledgments

This research was sponsored by the Austrian FWF under grants P12899 and P13778 as well as by a grant for an international joint research project from NEDO (Japan). The authors are grateful to the OEAD for support within the framework of the Austrian–French bilateral exchange programme Amadée, project V.9.

References

[1] Grytsiv A, Leithe-Jasper A, Flandorfer H, Rogl P, Hiebl K, Godart C and Velikanova T 1998 *J. Alloys Compounds* **266** 7
[2] Grytsiv A, Kaczorowski D, Leithe-Jasper A, Rogl P, Godart C, Potel M and Noël H 2002 *J. Solid State Chem.* **163** 37
[3] Massalski T B (ed) 1990 *Binary Alloy Phase Diagrams* 2nd edn (Materials Park, OH: ASM)
[4] Kranenberg C, Johrendt D and Mewis A 2001 *Z. Anorg. Allg. Chem.* **627** 539
[5] Rossi D and Ferro R 1996 *J. Alloys Compounds* **236** 212
[6] Kranenberg C, Johrendt D, Mewis A, Pottgen R, Kotzyba G, Trill H and Mosel B D 2002 *J. Solid State Chem.* **167** 107
[7] Merlo F, Pani M and Fornasini M L 1991 *J. Less-Common Met.* **171** 329
[8] Salamakha P, Demchenko P, Sologub O and Bodak O 1998 *J. Alloys Compounds* **278** 227
[9] Opanych I M 1996 *PhD Chemistry Thesis* Department of Inorganic Chemistry, L'viv State University
[10] Demchenko P, Bodak O and Muratova L 2002 *J. Alloys Compounds* **339** 100
[11] Andraka B, Petri R, Kaczorowski D, Leithe-Jasper A and Rogl P 2000 *J. Appl. Phys.* **87** 5149
[12] Petri R, Andraka B, Kaczorowski D, Leithe-Jasper A and Rogl P 2000 *Phys. Rev.* B **61** 12169
[13] Lebeau P and Figueras J 1903 *C. R. Acad. Sci., Paris* **136** 1329
[14] Elwell D and Scheel H J 1975 *Crystal Growth from High-Temperature Solutions* (London: Academic)
[15] Okada S, Atoda T, Higashim I and Takahashi Y 1987 *J. Mater. Sci.* **22** 2993
[16] Fisk Z and Remeika J P 1989 *Handbook on the Physics and Chemistry of Rare Earths* vol 12, ed A K Gschneidner and L Eyring (Amsterdam: Elsevier) p 53
[17] Roisnel T and Rodriguez-Carvajal J 2001 *Mater. Sci. Forum* **378–381** 118
[18] *Nonius Kappa CCD Program Package COLLECT, DENZO, SCALEPACK, SORTAV 1998 (Delft: Nonius)*
[19] Sheldrick G M 1997 *SHELX-97, Program for Crystal Structure Refinement* (University of Göttingen); Windows version by McArdle (National University of Ireland, Galway)
[20] Grytsiv A, Rogl P, Berger St, Paul Ch, Bauer E, Godart C, Ni B, Abd-Elmeguid M M, Saccone A, Ferro R and Kaczorowski D 2002 *Phys. Rev.* B **66** 094411
[21] Mader K H and Swift W M 1968 *J. Phys. Chem. Solids* **29** 1759
[22] Mott N F and Jones H 1958 *The Theory of the Properties of Metals and Alloys* (London: Oxford University Press)
[23] Rao V U S and Wallace W E 1970 *Phys. Rev.* B **2** 4613
[24] Yamada H and Takada S 1973 *J. Phys. Soc. Japan* **34** 51
[25] Maekawa S, Kashiba S, Tachiki M and Takahashi S 1986 *J. Phys. Soc. Japan* **55** 3194
[26] Fischer K H 1989 *Z. Phys.* B **76** 315
[27] Parthe E, Gelato L, Chabot B, Penzo M, Cenzual K and Gladyshevskii R 1994 *TYPIX Standardized Data and Crystal Chemical Characterization of Inorganic Structure Types* (Berlin: Springer)